Two-Component Droplet Wall-Film Interaction: Crown Morphology as a Function of Liquids Viscosity and Surface Tension

A. Geppert[1*], A. Štrbac[1], M. Marengo[2], G. Lamanna[1], B. Weigand[1]
[1]Institute of Aerospace Thermodynamics, University of Stuttgart, Stuttgart, Germany
[2]School of Computing, Engineering and Mathematics, University of Brighton, United Kingdom

Abstract

The study of single droplet impact onto thin films of a different liquid (two-component droplet wall-film interaction) has a great number of industrial applications like combustion processes, spray freeze drying or extinguishing film fuelled fires. In order to improve these applications the prediction of the number and size of the secondary droplets is essential. In this work special emphasis is given to the formation process of secondary droplets during crown-type splashing. In this process liquid jets (or fingers) develop along the upper rim, which later on break-up into secondary droplets. Hence, the first step for the prediction of secondary droplets is to predict the number of jets. Therefore, a systematic experimental study is carried out, employing low surface tension liquids ($\sim 28\, mN/m$) like n-Hexadecane and Hyspin. First, the splashing morphologies are linked to the characteristic crown parameters. Second, it is shown that the maximum number of liquid fingers from the liquid crown N_{max} is not a linear function of the crown rim radius. Instead, we present the dependency of N_{max} on experimental parameters like the non-dimensional film thickness ($0.1 < \delta < 0.5$) and the Weber number ($400 < We < 1700$). The dimensionless film thickness δ has the strongest influence. An increase in δ results in a decrease of the maximum number of liquid fingers N_{max}.

Keywords: drop dynamics, drop wall-film interaction, liquid properties

Introduction

The study of single droplet impact onto thin wall-films of a different liquid, the so called two-component droplet wall-film interaction, has a great number of industrial applications like spray freeze drying, extinguishing film fuelled fires or combustion processes. One example is the improvement of the carbon footprint of diesel engines. To reduce engine emission the exhaust gas temperature is increased by means of one or multiple post-injections. During the post-injection the piston moves downwards leaving the lubricating oil film on the chamber's wall exposed to the impinging diesel spray. The interaction between diesel droplets and oil wall-film may result in splashing, whereby secondary droplets, consisting of diesel and oil are ejected into the combustion zone. The combustion of secondary droplets containing oil would increase the engine emissions again. Hence, the development of a model, predicting the characteristics of these secondary droplets like number, size distribution and composition is necessary to improve the carbon footprint of diesel engines. Moreover, all above mentioned applications benefit from the detailed understanding of the physical mechanisms controlling the ejection of secondary droplets.

As a first step towards an understanding of these mechanisms the impact phenomenology of two-component droplet wall-film interaction needs to be determined and classified. But since the research on two-component droplet wall-film interactions is still in its early stages, only few publications can be found in the literature. The impact of water/glycerol droplets onto thin ethanol films was investigated by Thoroddsen et al. [1]. They focused on the mechanism of crown evolution and subsequent formation of holes in the crown wall. The latter they attribute to Marangoni-driven flows, which are triggered by local surface tension gradients, respectively concentration gradients. Banks et al. [2] published results of an experimental study on the effect of droplet and wall-film viscosity on the two-component droplet wall-film interaction. Employing water and aqueous solutions and focusing on a dimensionless film thickness of $\delta = h/D_0 = 1$, they found that the crown formation appears to be related more strongly to the wall-film properties, whereas crown splashing had some dependence on the droplet properties.

A first insight in the impact phenomenology of two-component systems consisting of alkanes, which are the liquids of interest for the present work, is presented in Geppert et al. [3]. Employing Hyspin and hexadecane as test liquids, they performed a comparative study between two- and one-component interactions. They found that the impact outcome, i.e. splashing and deposition, and the splashing morphology are similar for one- and two-component interactions. Furthermore, they are both dominated by the liquid properties of the wall-film. But, they also observed the formation of random holes in the crown wall.

Carrying on their investigations to deepen the previous findings, Geppert et al. [4] found that the impact morphology strongly depends on the liquids viscosity. The shape of the crown formed during impact turns from cylindrical for low-viscosity wall-films to conical for high-viscosity wall-films. The formation of holes in the crown wall is attributed to a non-uniform distribution of shear stresses, resulting from an inhomogeneous liquid

mixture and the viscosity gradient of droplet and wall-film liquid. As a first step towards a model predicting the properties of secondary droplets, they determined a correlation for the onset of splashing, which is valid for the Hyspin/hexadecane and the hexadecane/Hyspin interaction.

The present paper continues these investigations, giving special emphasis to the formation of secondary droplets during crown-type splashing. During this liquid fingers (or jets) develop along the upper crown rim and further break-up into secondary droplets. Hence, the prediction of the number of liquid fingers (or cusps) is a first step towards the prediction of the number of secondary droplets. A systematic experimental study, employing the low surface tension liquids Hyspin and hexadecane, is carried out. In this connection, the one- and two-component interactions of these liquids are investigated. The objective of this paper is twofold. First, we link the observed physical phenomena of crown-type splashing with the characteristic parameters of the crown, i.e. crown height, crown rim diameter and crown base diameter. Second, we show that the maximum number of liquid fingers N_{max} is not a linear function of the crown rim radius R_C and the correspondent rim disturbances wavelength λ, induced during droplet impinging. Instead, we found that experimental parameters like dimensionless film thickness δ, the Weber number of the droplet We and the liquid properties affect N_{max}.

Experimental Methods

The experimental set-up consists of three main parts: the droplet generation system, the impingement area and the two-perspective imaging system, which is the distinctive feature of the set-up. For the generation of droplets, having a diameter of $2.5\,mm$ and a maximum impact velocity of $4.5\,m/s$, a so-called dropper is employed. The impingement area consists of a smooth sapphire glass plate on which a thin metallic ring is glued. The resulting basin is filled with a measured amount of liquid, so that a wall-film of defined thickness is generated. The height of the wall-film is determined with a commercial device of the Micro-Epsilon company (Model: IFC2451 controller and IFS2405-3 sensor), that exploits the confocal chromatic imaging (CCI) technique. The error in the film height measurement was found to be less than 1% [5]. The two-perspective imaging system allows observing the droplet impact from two different viewing angles (lateral and front view) and hence to evaluate the impact symmetry. Therefore, the impingement area is illuminated from two directions and the respective shadowgraph images are then redirected, so that both images are projected next to each other onto the sensor of one Photron Fastcam SA1.1. The framerate of the camera was adjusted to $20{,}000\,fps$ and the shutter speed to $1/16{,}100\,s$. The resulting image size is $846\,x\,320\,pixel$. An image scale of 1:4 is employed to capture the complete impact process. To trigger the imaging system a laser light barrier is used. A detailed description of the experimental set-up and the operating procedure can be found in [5].

The properties of the droplet prior to impingement, i.e. droplet's diameter D_0 and impact velocity v_0, the parameter of the emerging crown (rim radius R_C, base radius R_{LB} and crown height H_C, which are depicted in Figure 1a and the number of liquid fingers N developing along the upper crown rim), are determined from the shadowgraph images. An image analysis program specifically written in MATLAB is used. The image analysis proceeds as follows. By using a graphical user interface the operator choose the experiment to be analysed and sets the boundary conditions, i.e. image section to be analysed (see Figure 1b), picture range for droplet analysis and crown analysis, minimum finger height, grey-scale threshold for transformation into binary image, liquid properties (density δ, viscosity μ and surface tension σ) and wall-film height h. The image analysis starts with post-processing the two-perspective pictures. In a first step the images are standardised by subtracting a background image. Next the pictures are cut into two partial pictures one for each perspective, according to the defined image sections. Finally they are transformed into binary images, taking into account the grey-scale threshold. An example of post-processed partial picture is shown exemplarily in Figure 1c. After this the following analysis steps proceed separately for each partial picture.

The diameter D_0 and the impact velocity v_0 of the droplet are determined from the consecutive images of the predefined picture range for droplet analysis. The final values are averaged over both partial pictures and the

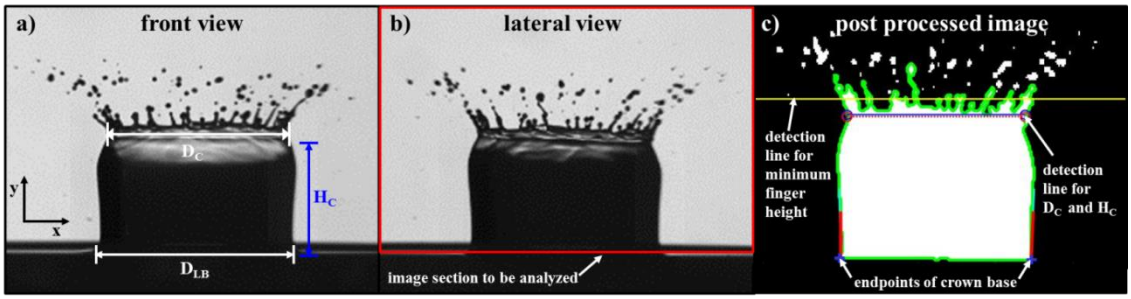

Figure 1a) and **b)**: two-perspective image of a crown developed at hexadecane one-component interaction ($\boldsymbol{We = 1320, \delta = 0.2}$), including definitions for the crown parameters $\boldsymbol{H_C}$, $\boldsymbol{D_C = 2R_C}$ and $\boldsymbol{D_{LB} = 2R_{LB}}$ in a) and example for the image section to be analyzed in b). **c)**: lateral view after post-processing, including explanations for different detection points.

complete picture range. The uncertainty in D_0 and v_0 was predicted to be 2% [5]. For the comparison of the experimental results the following characteristic dimensionless numbers are calculated, using D_0, v_0, the wall-film height h and the liquid properties of the droplet (ρ_D, μ_D, σ_D) and the wall-film (ρ_F, μ_F, σ_F): the dimensionless film thickness $\delta = h/D_0$, the Weber number of the droplet $We_D = \rho v_0^2 D_0/\sigma_D$ and the Ohnesorge number of droplet $Oh_D = \mu_D/\sqrt{D_0 \rho_D \sigma_D}$ and the wall-film $Oh_F = \mu_F/\sqrt{h \rho_F \sigma_f}$. For these numbers the uncertainty was determined to be 2.5%, 5% and 3% [5], respectively. The non-dimensional time, relative to the moment of droplet impact on the wall-film, is defined as $T = t v_0/D_0$.

The analysis of the crown parameters is carried out as follows for each partial picture of the corresponding predefined picture range for crown analysis. As a first step the *x* and *y* values of the crown contour for every line of pixel are determined (see green contour line in Figure 1c) and stored into an array of data (contour data). At the bottom of the crown contour (first 5 rows of contour data) the endpoints of the lamella base are determined (see Figure 1c) and the diameter of the lamella base D_{LB} is calculated as the difference in their *x*-coordinates. The corresponding *y*-value for the lamella base is later on used to determine the crown height. The location of the crown rim is determined by analysing for each line of pixel the number of side by side located white pixels. At the upper crown rim, where the fingers emerge, the line of side by side located pixels is disturbed. Hence, the last line of undisturbed pixels is defined as crown rim (see Figure 1c). Here again the endpoints are determined and the subtraction of their *x*-values gives the crown rim diameter D_C. The height of the crown H_C is determined by subtracting the *y*-values of crown rim and crown base. For the counting of the liquid fingers the predefined minimum finger height l_{min} is added to the crown height, so that a minimum detection height (represented by the yellow line in Figure 1c) is defined. All lines of pixel above this detection height are searched for their number of liquid fingers. The largest number of liquid fingers is defined as the maximum number of liquid fingers per picture $N_{pic,max}$. The determined values for D_{LB}, D_C, H_C and $N_{pic,max}$ for each partial picture and for each time step, are stored in a second data array (crown parameters). The total maximum number of liquid fingers N_{max} for each experiment is defined as the maximum of $N_{pic,max}$ of each partial picture and each time step. The uncertainty of the count of fingers was determined by comparing the number of finger resulting from the image analysis program with a manual counting. It was found to be ± 2 fingers.

In the present work the one-component interactions of Hyspin AWS 10 (hydraulic oil) and n-Hexadecane $C_{16}H_{32}$, long-chain alkane) and the two-component interactions (droplet liquid/wall-film liquid) of Hyspin/hexadecane and hexadecane/Hyspin are investigated. The physical properties of these low surface tension liquids are summarized in Table 1. Note that the viscosity of Hyspin is more than four times larger than that of hexadecane, while the remaining liquid properties are similar.

Table 1 Physical properties of the test liquids

	dyn. viscosity μ $[Pa\ s]$	surface tension σ $[mN/m]$	density ρ $[kg/m^3]$
Castrol Hyspin AWS 10	0.01580	28.65	878
n-Hexadecane	0.00345	27.52	773

A systematic study was carried out for a wide range of experimental conditions: $0.1 < \delta < 0.5$, $400 < We < 1700$, $0.013 < Oh_D < 0.07$ and $0.020 < Oh_F < 0.220$. In practice, the wall-film thickness was varied and the droplet diameter kept constant to achieve different values for dimensionless film thickness δ. The Weber number was varied by changing the droplets fall height, hence its final velocity.

Experimental results

Physical Phenomena

The splashing morphology for the investigated two-component (first and second row) and one-component interactions (third and fourth row) is shown exemplarily for $\delta = 0.2$ and $We > 1300$ in Figure 2. The image sequences of all four cases show the crown-type splashing, with its characteristic development of liquid fingers along the crown rim and their subsequent break-up into secondary droplets. The first picture of every sequence shows the crown evolution at an early stage after impact ($T < 3$). Looking at the Hyspin/hexadecane interaction (1a), disturbances along the crown rim are clearly visible, while for the hexadecane/Hyspin interaction (2a) the crown rim is almost undisturbed. This effect is even more pronounced for the one-component interactions. For the low-viscosity liquid hexadecane (3a) the development of fingers has already started, whereas for the high-viscosity liquid Hyspin (4a) the crown rim is still undisturbed. Hence, an increase of wall-film viscosity results in a delayed onset of fingering. Considering the second picture of each sequence, this is further supported by the fact that for Hyspin/hexadecane (1b) and the hexadecane one-component interaction (3b) the liquid fingers already break-up into secondary droplets at $T \approx 6$, while for hexadecane/Hyspin interaction (2b) and the Hyspin one-component interaction (4b) this process just starts. Furthermore, staying at the first two pictures of the Hyspin/hexadecane (1a, 1b) and hexadecane one-component interaction (3a, 3b), it can be seen that not all dis-

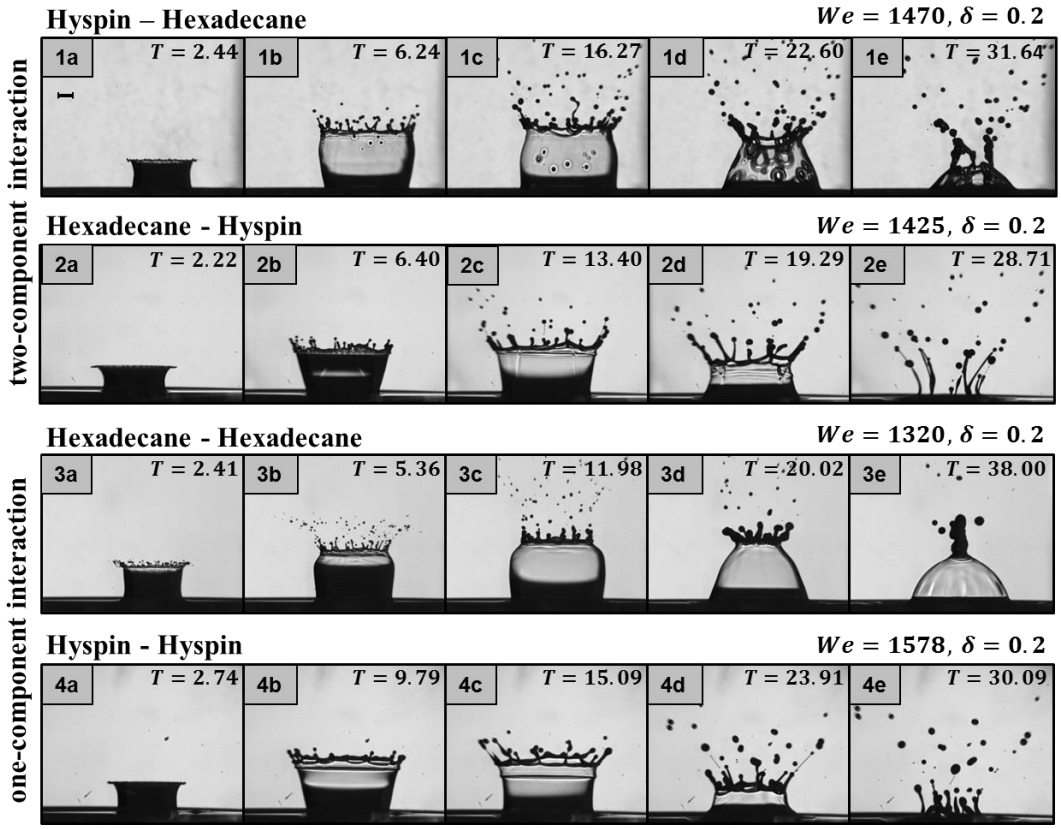

Figure 2 Exemplary image sequences for the morphologies of crown-type splashing observed for the investigated two-component (row 1 and 2) and one-component (row 3 and 4) interactions for $\boldsymbol{\delta = 0.2}$ and $\boldsymbol{We > 1300}$. The values in the upper right corners give the non-dimensional time after impact.

turbances emerging during the early stage of crown evolution later on grow into liquid fingers. Hence, for the correct detection of the number of liquid fingers a minimum finger height l_{min} has to be defined to exclude these disturbances from the counting. The determination of this value l_{min} is described below. Looking at the remaining three pictures (c-e) of every sequence, the difference in crown shape and evolution, depending on the liquid properties, is clearly visible. The Hyspin/hexadecane crown develops a cylindrical shape during the ascending phase (1b). In the receding phase the crown rim starts to contract (1c). As a result, the liquid fingers are melted together (1d) until the crown finally collapses (1e). By contrast, the crown formed during hexadecane/Hyspin interaction has a V-shaped (or conical) contour (2b) that is preserved during the receding phase (2c-d). The liquid fingers are elongated during crown receding and persist after the descent of the crown (2e). Comparing these two-component impact morphologies with the one-component ones, a similarity between the Hyspin/hexadecane interaction and the hexadecane one-component interaction as well as between the hexadecane/Hyspin interaction and the Hyspin one-component interaction can be noted. The hexadecane one-component interaction shows a cylindrical crown shape (3b) and a strengthened crown rim contraction (3d), leading to the formation of a closed bubble (3e). In comparison, the Hyspin one-component interaction reveals a V-shaped crown (4b) and also the liquid fingers persist after crown descent (4e). It can be therefore concluded that the properties of the wall-film strongly influence the impact morphology of the two-component interactions. This is in accordance with previous findings presented by Geppert et al. [4] for $\delta = 0.1$ and $We = 1000$. Besides, the observed differences in the receding phase of the crown make it necessary to limit the counting of liquid fingers before crown collapse or complete crown rim contraction (prior to pictures 1e-4e in Figure 2). Otherwise results are not comparable.

Crown characteristics

In this paragraph the previously described physical phenomena are linked to the characteristic parameters of the crown and their evolution during the impact process. The considered crown parameters are the radius at the upper rim of the crown $R_C = D_C/2$, the height of the crown H_C and the radius at the base of the crown $R_{LB} = D_{LB}/2$ (cf. Figure 1). In Figure 3 the evolution of the crown rim radius R_C (upper graph) and the crown height H_C (lower graph) are depicted exemplarily for the experiments shown in Figure 2. To allow a correct comparison of the results, the crown parameters are made dimensionless with the diameter of the impinging droplet D_0 and they are plotted against the dimensionless time $T = tv_0/D_0$.

In general, the evolution of the crown rim radius R_C/D_0 follows a parabolic trend with time, which means that

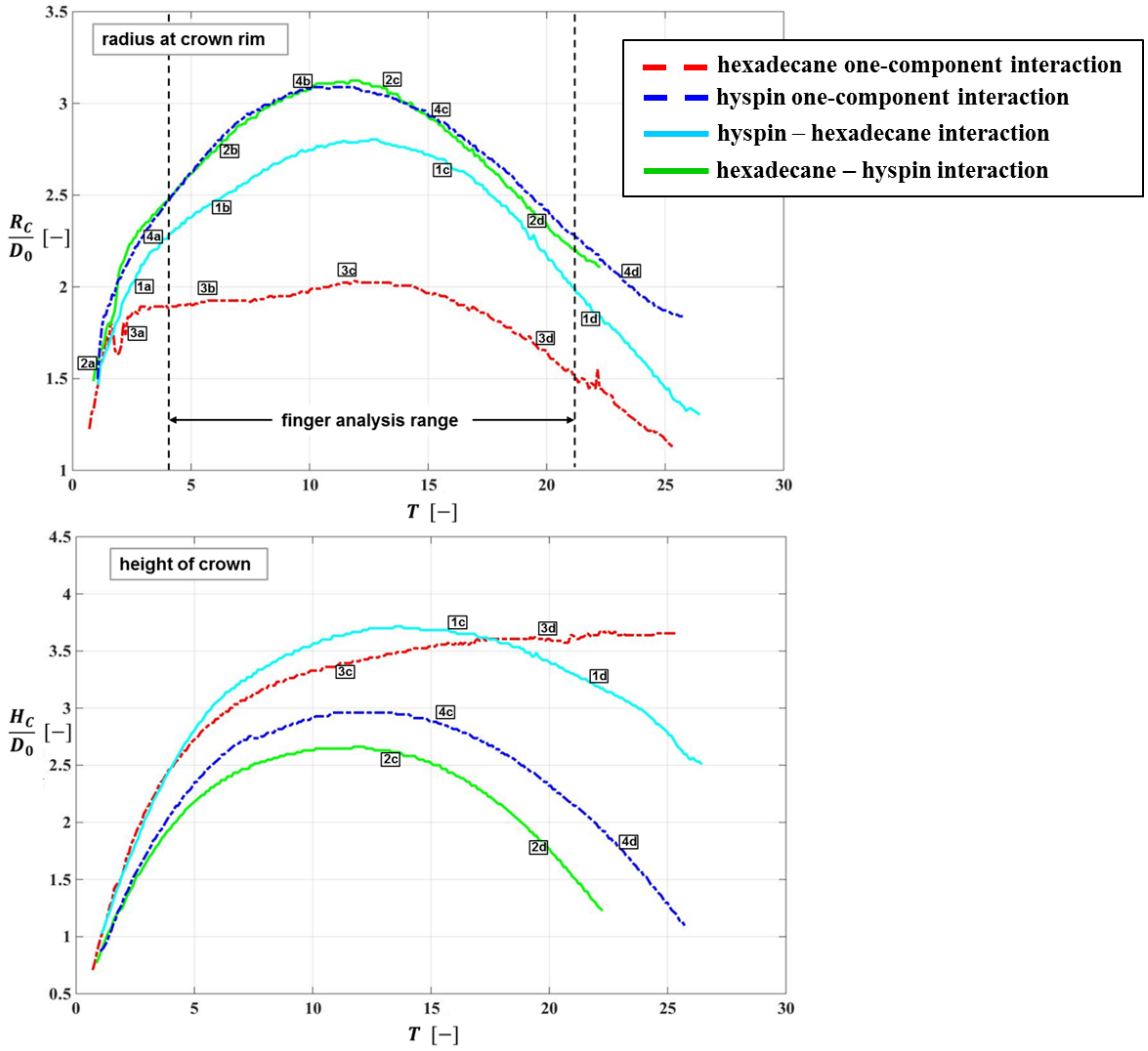

Figure 3 Exemplary plots of the characteristic crown parameters $\boldsymbol{R_C/D_0}$ (upper graph) and $\boldsymbol{H_C/D_0}$ (lower graph) as a function of dimensionless time $\boldsymbol{T = tv_0/D_0}$ for the experimental cases discussed in the previous paragraph. The encapsulated numbers refer to the corresponding images in Figure 2.

R_C/D_0increases until it reaches a maximum radius $(R_C/D_0)_{max}$ and then decreases again. The liquid properties, especially the viscosity of the wall-film, influence the height and the width of the curves. Considering the two-component interactions, it can be seen that for the hexadecane/Hyspin interaction (green line) $(R_C/D_0)_{max}$ is larger and is reached at an earlier point in time, compared to the Hyspin/hexadecane interaction (cyan line). In this case $(R_C/D_0)_{max}$ is smaller and it is reached at a later point in time. That implies that a decrease in wall-film viscosity results in a decrease in $(R_C/D_0)_{max}$ and shifts this maximum to later points in time. Furthermore, this effect is linked to the observed crown shapes (cf. Figure 2). The V-shaped crown of hexadecane/Hyspin interaction promotes the growing of R_C/D_0, whereas the cylindrical shape and the crown rim contraction observed during Hyspin/hexadecane interaction restrict it. A comparison between the Hyspin one-component interaction (blue line) and the hexadecane one-component interaction (red line) shows this effect even more pronounced. For the low-viscosity liquid hexadecane, the growth of R_C/D_0 passes two different stages. At the beginning ($T < 3$) R_C/D_0 grows rapidly and with a comparable rate of growth as in the other cases. But for $T > 3$ the growth rate of R_C/D_0 slows down dramatically and nearly stagnates. For the high-viscosity liquid Hyspin a parabolic progression for R_C/D_0 is observed. Note that to reach a comparable R_C/D_0 as at the hexadecane/Hyspin interaction ($We = 1420$), the hypsin one-component interaction requires a larger amount of kinetic energy ($We = 1578$). In the upper graph of Figure 3 the evaluation range for the number of liquid fingers is marked, too.

The evolution of the dimensionless crown height H_C/D_0 is shown in the lower graph of Figure 3. Regarding the curve progression of the dimensionless crown height H_C/D_0 again a parabolic shape is observed, except for the hexadecane one-component interaction, which shows an asymptotic progress. This is strongly linked to the observed impact morphologies. Since for the hexadecane one-component interaction the formation of a closed bubble was observed, the asymptotic value of the crown height is the maximum height of the bubble, which is

reached at the moment the crown rim contraction finishes. The parabolic shape reproduces the advancing and receding of the crown as it is depicted in Figure 2 for the hexadecane/Hyspin, Hyspin/hexadecane and Hyspin one-component interaction. Looking at the height evolution of the two-component interactions, we see that the crown rim contraction observed for the Hyspin/hexadecane interaction (cyan line) decelerates the receding of the crown, which leads to a wider opening angle of the curve, compared to the hexadecane/Hyspin curve. This effect is more pronounced for the hexadecane one-component interaction, where the strengthened crown rim contraction, hence the formation of a bubble, inhibits the receding of the crown. A comparison of the maximum crown heights $(H_C/D_0)_{max}$ for the two-component interactions (green and cyan line) shows that with increasing wall-film viscosity the crown height decreases. The same trend is observed for the one-component interactions. Despite the higher impact energy of the Hyspin one-component interaction ($We = 1578$), its maximum crown height ($(H_C/D_0)_{max} = 3$) stays below the maximum height achieved at the hexadecane one-component interaction ($We = 1320$, $(H_C/D_0)_{max} = 3.7$). Note that the maxima for $(H_C/D_0)_{max}$ and $(R_C/D_0)_{max}$ are reached at the same point of time for all cases, but for the hexadecane one-component interaction.

Finally, the evolution of the radius at the crown base R_{LB}/D_0 (not depicted here) is considered. A comparison of the curve progressions of all four cases shows that up to $T = 2$, they have the same tendency. This means that at this early stage the growing of R_{LB}/D_0 is independent of the liquid properties. Due to the higher viscosity of the wall-film, the rate of growth is slowed down at later times for the cases of hexadecane/Hyspin and Hyspin one-component interaction. Moreover, the maximum $(R_{LB}/D_0)_{max}$ for these cases is smaller compared to the Hyspin/hexadecane and hexadecane one-component interactions, which have a low-viscosity wall-film. Hence, an increase in wall-film viscosity leads to a decrease in $(R_{LB}/D_0)_{max}$.

In summary, an increase in wall-film viscosity leads to a decrease in $(R_{LB}/D_0)_{max}$ and $(H_C/D_0)_{max}$, but to an increase in $(R_C/D_0)_{max}$. This is because with increasing wall-film viscosity the angle between crown and wall-film decreases, changing the direction of propagation of liquid from vertical to inclined. This causes the differences in crown shape, i.e. cylindrical or V-shaped. Hence, depending on the wall-film viscosity the remaining energy is either used to increase the crown height (low viscosity) or the crown rim radius (high viscosity). This influences the formation of liquid fingers along the crown rim and explains the time shift for the onset of fingering.

Analysis of maximum number of liquid fingers N_{max}

In this paragraph the results of the analysis of the maximum number of liquid fingers N_{max}, developed during crown-type splashing of the considered liquid combinations, are presented.

A mentioned before, it is necessary to define a minimum finger height l_{min} to ensure a correct counting of fingers. Therefore, the progression of N up to N_{max} was evaluated for different l_{min} between $2 < l_{min} < 7$ and compared to a manual counting for selected experiments. The best agreement was achieved for $l_{min} = 5$, which is in the following used to perform the analysis.

The first approach for the development of a correlation predicting N_{max}, is to link N_{max} with the characteristic parameters of the crown, i.e. the crown rim radius R_C. Therefore, we used a geometrical approach where N_{max} is defined as the perimeter of the crown ($2\pi R_C$) divided by the wavelength of the disturbances λ, induced during

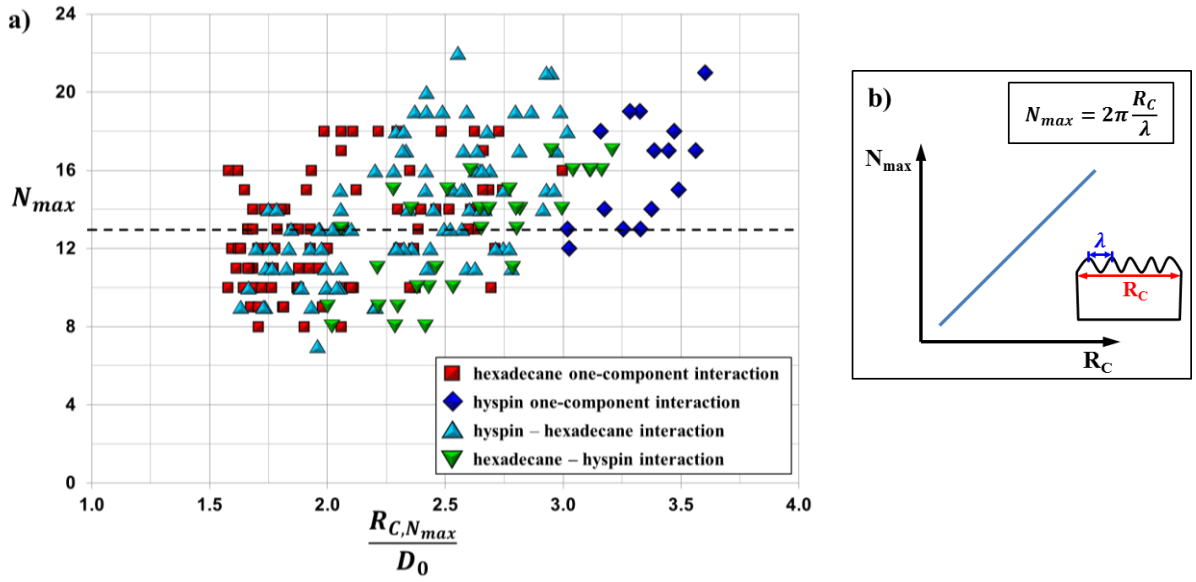

Figure 4a): Maximum number of liquid fingers N_{max} plotted against the dimensionless crown rim radius $R_{C,N_{max}}/D_0$ at the time of N_{max} for all analyzed experiments. **b)**: Schematic drawing for explanation of linear dependence between N_{max} and R_C for a constant disturbance wavelength λ.

droplet impingement (cf. Figure 4b). Besides, the wavelength λ is assumed to be constant neglecting the damping force resulting from liquid viscosities. Hence, N_{max} should depend linearly on R_C as schematically depicted in Figure 4b. Therefore, a larger number of liquid fingers for a larger crown rim radius is expected. But looking at the experimental results in Figure 4a shows that this is not the case. In Figure 4a N_{max} is plotted against the dimensionless crown rim radius $R_{C,N_{max}}/D_0$, measured at the time of N_{max}. Note that, in general the maximum number of fingers is between $7 < N_{max} < 22$, for all considered experiments. But at first glance, it is obvious that due to the scatter of the results, N_{max} is not a linear function of the crown parameter $R_{C,N_{max}}/D_0$. Regarding the black dashed line in the graph, which exemplarily marks $N_{max} = 13$, it can be seen that for all four liquid combinations this number of liquid fingers is observed for different crown rim radii. Moreover, already the impact morphologies presented in Figure 2 show that a larger crown rim diameter not necessarily leads to a larger number of liquid fingers (compare row 1 to row 2 or row 3 to row 4). This means that, the disturbance wavelength λ is not constant for the considered experimental parameter range.

To clarify this, we looked how the experimental parameters, influencing the impact outcome, affect the maximum number of liquid fingers N_{max}. The influence of the wall-film thickness is described by the dimensionless film thickness δ. The Weber number characterizes the influence of the droplet's impact energy and the Ohnesorge number describes the influence of the liquid properties of droplet and wall-film. In the following their influences on N_{max} are considered separately. The most pronounced influence on N_{max} was determined for the dimensionless film thickness δ. In Figure 5 the maximum number of fingers N_{max} is plotted against δ, for every investigated one- and two-component interaction. The symbols give the average number of liquid fingers counted for one value of δ. In this averaging process the potential influence of all other parameters is disregarded. The error bars represent the scatter range of the experiments. Note that the sparse data set for the Hyspin one-component interaction (graph in lower, left corner of Figure 5) results from the fact that, to induce splashing for this liquid for $\delta \geq 0.3$ requires $We > 1800$, which exceed the capability of our experimental test rig.

For all investigated liquid combinations N_{max} decreases with increasing δ. This means a thicker wall-film stronger damps the finger formation. That is explained by the fact that for the displacement of a thicker wall-film more energy is dissipated, which is later on not available for the finger formation. Regarding the scatter range, which is in most cases larger than the uncertainty of finger counting of ± 2, there must be further parameter affecting N_{max}. It appears likely that the available impact energy, respectively the Weber number, has an effect on N_{max}. In general, we found that an increase in Weber number results in a slight increase in N_{max}, but up to now our data are too sparse to identify a justifiable trend and therefore the results are not presented here.

Finally, the influence of the liquid properties on the maximum number of fingers N_{max} is presented. Therefore,

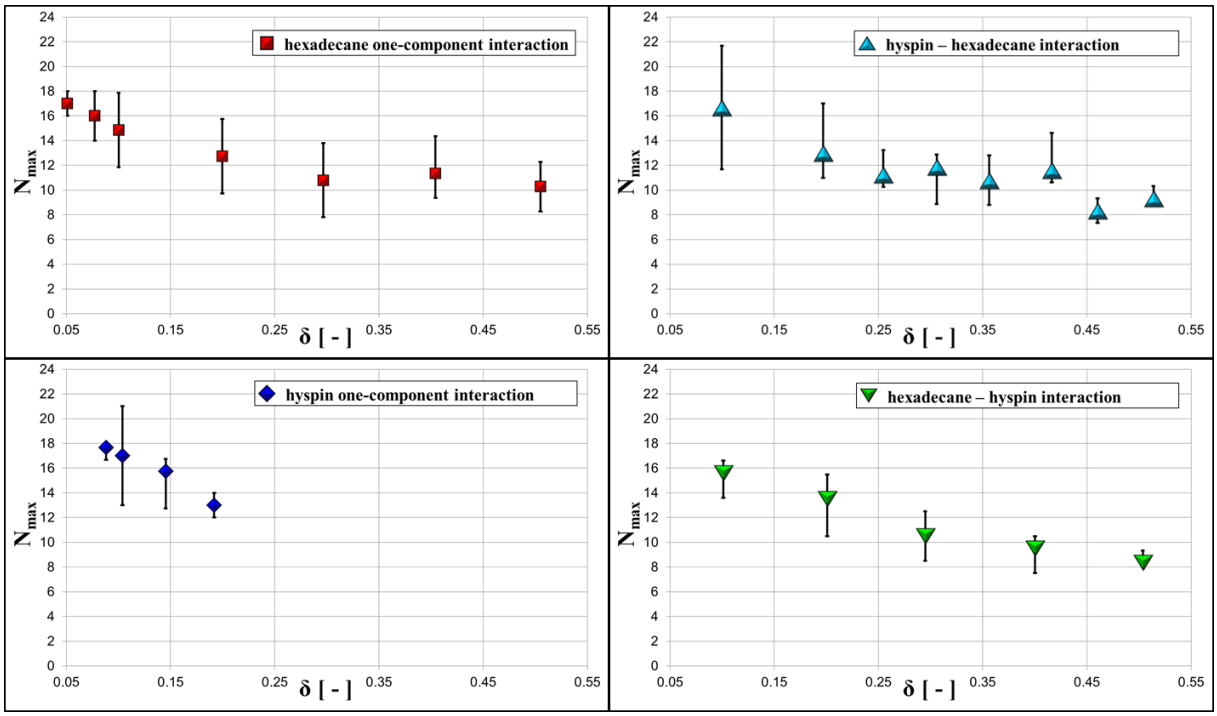

Figure 5 The maximum number of liquid fingers N_{max} is plotted against the dimensionless film thickness δ for hexadecane and Hyspin one-component interactions on the left-hand side and for the two-component interactions (Hyspin/hexadecane and hexadecane/Hyspin) on the right-hand side. The average is including all Weber numbers. The symbols represent the average number of fingers and the error bars represent the scatter range of the experiments.

we introduce a specific Ohnesorge number $Oh_{\bar{\mu},\delta} = \frac{0.5(\mu_F+\mu_D)}{\sqrt{\delta\rho_D\sigma_D}}\frac{1}{\sqrt{D_0}}$, which is based on the averaged viscosity of droplet and wall-film, the droplet's density and surface tension (cf. Table 1) and the dimensionless film thickness δ. To be precise, this $Oh_{\bar{\mu},\delta}$ combines the influence of the liquid properties and δ. In Figure 6 the resulting plot for N_{max} against $Oh_{\bar{\mu},\delta}$ is shown. Looking at one liquid combination an increase in $Oh_{\bar{\mu},\delta}$ due to a decrease in δ, shows an increase in N_{max}, as described previously. Furthermore, an increase in $Oh_{\bar{\mu},\delta}$ due to an increase in liquid viscosity, results in an increase of N_{max}, but this dependency is rather weak.

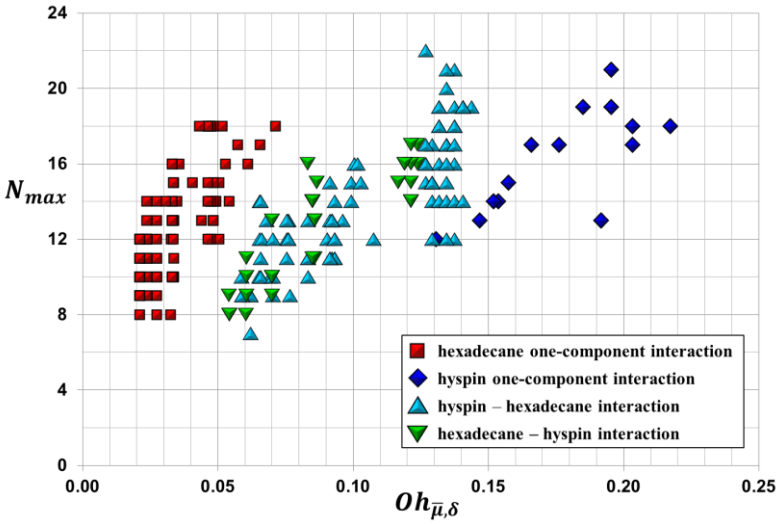

Figure 6 The maximum number of liquid fingers N_{max} is plotted against the specific Ohnesorge number $Oh_{\bar{\mu},\delta} = (0.5(\mu_F + \mu_D)/\sqrt{\delta\sigma_D\rho_D}) \cdot 1/\sqrt{D_0}$ for all considered experiments.

Conclusions

To improve industrial applications like spray freeze drying, extinguishing film fuelled fires of combustion processes the physical mechanism controlling the ejection of secondary droplets needs to be understood. Therefore, in the present work special emphasis is given to formation of liquid fingers along the upper crown rim during crown-type splashing. Since these fingers later on break-up into secondary droplet, the prediction of their number is a first step towards predicting the number of secondary droplets. In this work the finger formation is investigated for the one- and two-component interactions of Hyspin and hexadecane. First, we linked the observed splashing morphologies with the characteristic crown parameters R_C, R_{LB} and H_C. We found that an increase in wall-film viscosity leads to a decrease in R_{LB} and H_C, but to an increase in R_C. This is linked to the energy dissipation in the wall-film that is responsible for the cylindrical crown shape of low-viscosity liquids and the conical crown shape for high-viscosity liquids. Moreover, the maxima for R_C and H_C are reached at the same instant for all considered liquid combinations except the hexadecane one-component interaction. Here, the bubble formation strongly alters the impact morphology and the evolution of characteristic crown parameters. In a second step we presented the dependency of the maximum number of liquid fingers N_{max} on the experimental parameters δ, We and $Oh_{\bar{\mu}\delta}$, because an attempt to link N_{max} to the crown rim radius R_C showed no justifiable tendency. We found that for all considered liquid combinations an increase in δ results in a decrease in N_{max}. In contrast, an increase in $Oh_{\bar{\mu}\delta}$ due to an increase in viscosity, results in an increase in N_{max}, even if this dependency is only weak. For the influence of We on N_{max}, no justifiable trend could be defined because our data sets were to sparse but, since the surface tension was not varied, a variation of the Weber number is mainly linked of the impact velocity only. In general, we observed that an increase of impact velocity results in a slight increase of N_{max}.

Acknowledgements

The authors kindly acknowledge the financial support of this work by the Deutsche Forschungsgemeinschaft (DFG).

References

[1] Thoroddsen, S. T., Etoh, T. G., and Takehara, K., *Journal of Fluid Mechanics* Vol. 557: 63-72 (2006).
[2] Banks, D., Ajawara, C., Sanchez, R., Surti, H., and Aguilar, G., *Atomization and Sprays* 23 (6): 524-540 (2013).
[3] Geppert, A., Greif, F., Lamanna, G., and Weigand, B, *25th European Conference on Liquid Atomization and Spray Systems ILASS*, Chania, Greece, 1-4 September, 2013.
[4] Geppert, A., Gomaa, H., Meister, C., Lamanna, G., and Weigand, *Americas 26th Annual Conference on Liquid Atomization and Spray Systems*, Portland, Oregan, USA, 18-21 May, 2014.
[5] Geppert, A., Chatzianagnostou, D., Meister, C., Gomaa, H., Lamanna, G., and Weigand, B., *Atomization and Spray*, accepted for publication, 2015.